ACS Catalysis

Research Article

pubs.acs.org/acscatalysis

Counterion Effect in the Reaction Mechanism of NHC Gold(I)-Catalyzed Alkoxylation of Alkynes: Computational Insight into Experiment

Gianluca Ciancaleoni,[†] Leonardo Belpassi,[†] Daniele Zuccaccia,[†,‡] Francesco Tarantelli,[†,§] and Paola Belanzoni*[,†,§]

[†]Istituto di Scienze e Tecnologie Molecolari del CNR (CNR-ISTM), c/o Dipartimento di Chimica, Biologia e Biotecnologie, Università degli Studi di Perugia, via Elce di Sotto 8, I-06123, Perugia, Italy

[‡]Dipartimento di Chimica, Fisica e Ambiente, Università di Udine, Via Cotonificio 108, I-33100 Udine, Italy

[§]Dipartimento di Chimica, Biologia e Biotecnologie, Università degli Studi di Perugia, Via Elce di sotto 8, I-06123, Perugia, Italy

Supporting Information

ABSTRACT: Experimental data suggest that anions that provide a compromise between the hydrogen-bond acceptor and the coordinating powers rather than poor coordinating anions unexpectedly increase the efficiency of L–Au–X (L = ligand, X = anion) catalyzed alkyne alkoxylation reactions, where the nucleophilic attack is the rate-determining step. No systematic computational studies about the role of the anion in the different steps of the catalytic cycle are available yet. In this paper, the remarkable anion influence on the catalytic efficiency of [NHCAuX] (X = BF_4^-, OTf^-, OTs^-, TFA^-, and OAc^-) complexes in the intermolecular addition of methanol to 2-butyne process has been analyzed through a density functional theory (DFT) approach. The role of the anion has been considered in all the steps of the reaction mechanism: pre-equilibrium, nucleophilic addition, and protodeauration. In the nucleophilic attack step, the anion acts (i) as a template, holding the methanol in the right position for the outer-sphere attack; (ii) as a hydrogen-bond acceptor, enhancing the nucleophilicity of the attacking methanol; (iii) as catalyst deactivator, by either its strong coordinating and/or basicity power, preventing the alkyne coordination or forming free alkoxide, respectively. In the protodeauration step, the anion acts as a proton shuttle, lowering the activation barrier. DFT calculations support intermediate coordinating and basicity power anions as the most efficient catalysts.

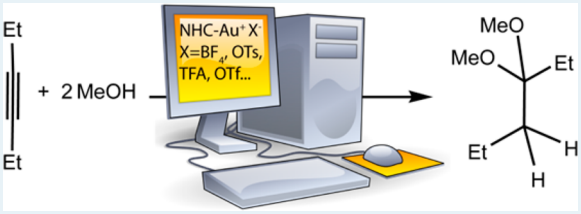

KEYWORDS: *alkynes, DFT calculations, homogeneous catalysis, N-heterocyclic carbene–gold complexes, reaction mechanism, anion effect*

INTRODUCTION

For a long time gold was considered a noble, seemingly inert metal, while, nowadays, gold catalysis is acknowledged as one of the hot topics in current organic synthesis.[1] The "catalytic gold-rush" started about 20 years ago with the discovery that gold can efficiently catalyze the addition of nucleophiles, such as water or methanol, to alkynes.[2] Since the beginning the anion effect on catalytic performances was observed,[3] and together with the ligand effect,[4] the anion was recognized to be important in tuning the catalytic performances, as the activity,[5] the regioselectivity[6] and the stereoselectivity.[7]

Among the gold-catalyzed processes, the alkoxylation of alkynes is still the most investigated one.[8] A general accepted mechanism[9] was proposed, consisting of the following steps: the active species [L_nAu] coordinates and activates the alkyne toward the nucleophile attack by methanol,[10] then the reaction is completed by the anion- or solvent-assisted[11] proton transfer from the methanol OH group to the other carbon atom (protodeauration), forming an enol-ether product. Subsequent reaction of the enol-ether with a second methanol molecule leads to the formation of the acetal final product, probably through a classical acid-catalyzed process.[12] Despite the large amount of work on the methanol addition to alkynes, systematic experimental studies aimed at understanding the role of the anion are only very recent,[13,14] while, from the theoretical point of view, to the best of our knowledge, no systematic computational data are available yet.

Up to now, the role of the anion has been firmly recognized only in the protodeauration step, acting as a proton shuttle, or forming weak interactions with the substrate in order to explain the enantioselectivity,[15] or modulating the reactivity of cationic intermediates,[16] whereas the anion effect in the nucleophilic attack step has been analyzed only in our preliminary communication.[14] A rational understanding of anion effects in gold catalysis is therefore lacking, particularly in the light of new experimental results.[13,14]

Received: October 30, 2014
Revised: December 17, 2014
Published: December 18, 2014

DOI: 10.1021/cs501681f
ACS Catal. 2015, 5, 803–814

In a series of experiments on gold-catalyzed alkoxylation of alkynes, some of the present authors have found that [IPrAuX] (IPr = 1,3-bis(2,6-di-isopropylphenyl)-imidazol-2-ylidene, X = BAr^{F-} (tetrakis(3,5-bis(trifluoromethyl)phenyl)-borate), BF_4^-, OTf^- (trifluoromethanesulfonate), OTs^- (*p*-toluensolfonate), TFA^- (trifluoroacetate), or OAc^-(acetate)) is an efficient catalyst, with the activity depending on the nature of the anion. For this reaction the authors have carried out a series of kinetic experiments using CH_3OH as nucleophile, 3-hexyne as substrate and $CDCl_3$ as solvent (see Scheme 1).

Scheme 1. Schematic Representation of the Experimentally Studied Reaction

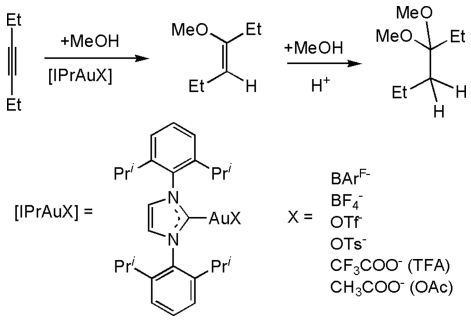

Experimental results show that the order of catalytic efficiencies is the following: OTs^- > OTf^- > BF_4^- > BAr^{F-} > TFA^-, with the OAc^- showing no catalytic activity (Figure 1).

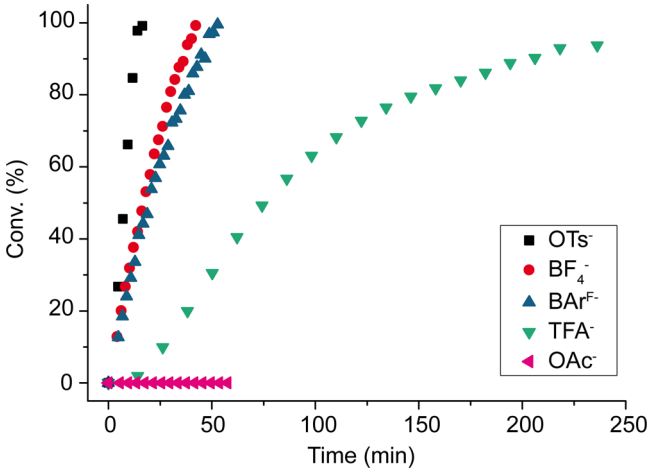

Figure 1. Alkoxylation of 3-hexyne with [IPrAuX] catalysts.

Very surprisingly, the activity trend does not match with the coordinating ability of the anions, which increases in the order: BAr^{F-} < BF_4^- < OTf^- < OTs^- < TFA^- < OAc^-.[17,11b] This counterintuitive or unexpected result (since weak coordinating anions are commonly chosen as anion in homogeneous gold catalysis in order to enhance the catalyst efficiency) deserves detailed investigation on the role of the anion in the reaction mechanism. Noteworthy, also in the work of Zhdanko and Maier (carried out in CD_2Cl_2 and with PPh_3 and *o*-(di-*tert*-butylphosphino)-biphenyl as ligands)[13] the OTs^- has been shown to significantly enhance the catalytic performances of the gold catalyst.

In the catalytic conditions employed by Zuccaccia et al.[14] the nucleophilic attack of the first methanol molecule has been determined to be the rate-determining step, thus suggesting an active role of the anion within this step.

The mechanism proposed by us combining theoretical and experimental findings is summarized in Scheme 2. The role of the anion is emphasized in all the steps of the pathway, which are the pre-equilibrium, the nucleophilic attack of methanol to the Au−butyne complex (step I) and the proton transfer to the unsaturated carbon atom (protodeauration, step II). For the latter, the role of the anion has been already explored,[11b] while in the former two beneficial roles of the anion can be envisaged: (i) it holds the reactive methanol molecule in the right position for an anti-periplanar (outer-sphere[10]) addition, acting as a template ($\mathbf{RC_X}$ structure, Scheme 2); (ii) it enhances the nucleophilicity of the attacking methanol through the MeOH···X^- hydrogen bond (HB), which induces a larger polarization on the oxygen. The importance of HBs in gold-catalyzed process has been also established in recent works showing the influence of HB acceptors and donors on the catalytic output.[5a,18,19]

Step I, however, can be disrupted by an anion-induced catalyst poisoning, through two possible deactivation pathways: a strongly coordinating anion will shift the pre-equilibrium stronger to the left (i.e., toward $\mathbf{IC_X}$), eventually forming an intermediate tricoordinated complex, [NHCAuX(2-butyne)]-(MeOH) ($\mathbf{TC_X}$, Scheme 2); alternatively, a strongly basic anion can abstract a proton from the methanol, leading to the formation of the corresponding acid HX and free MeO^-, which deactivates the catalyst through the formation of the catalytically inactive species (deactivated complex, $\mathbf{DC_X}$, see Scheme 2 and ref 14). Actually, the presence of [NHCAuOMe] has been experimentally observed when TFA^- was used as anion.[14]

In this paper, we report a density functional theory (DFT) description of the first methanol molecule addition, since experimental evidence for a faster second methanol molecule addition to vinyl ether has been given.[5a]

Complex [NHCAuX] (NHC = 1,3-dimethylimidazol-2-ylidene; X = OTs^-, BF_4^-, OTf^-, TFA^-, and OAc^-) has been chosen as a model for the catalytically active species, 2-butyne and methanol have been selected as substrate and nucleophile, respectively, for the calculations (Scheme 3). The influence of the above anions on the catalytic efficiency of [NHCAuX] complexes in the methanol addition to 2-butyne process under examination has been thoroughly analyzed, resulting in a tunable interplay between the coordinating ability and the hydrogen bonding acceptor properties of the anion with respect to methanol.

We should mention here that preliminary DFT calculations have been performed by us on the reaction mechanism of Scheme 2 using OTs^- as an anion in ref 14, where the experimentally observed anion effect has been rationalized on the basis of the coordinating and basicity properties of this anion. Its best catalytic performance has been attributed to its ability to abstract the proton from the methanol and thus to its basicity.[14] In this paper we have extended our analysis to all the experimentally used anions and to more subtle effects.

In order to elucidate the anion role on the reaction mechanism, we decided to include in our analysis the bare $[NHCAu]^+$ complex, without any anion. This could be a good model when a polar solvent is used (methanol itself, for example) or in the presence of very low coordinating anions, such as BAr^{F-},[20] which is known to prevent the ion pairing phenomenon, at least at low concentration.[21]

DOI: 10.1021/cs501681f
ACS Catal. 2015, 5, 803−814

Scheme 2. Reaction Mechanism between 2-Butyne and Methanol Catalyzed by the [NHCAuX] Complex Showing the Role of Anion X^{-}[a]

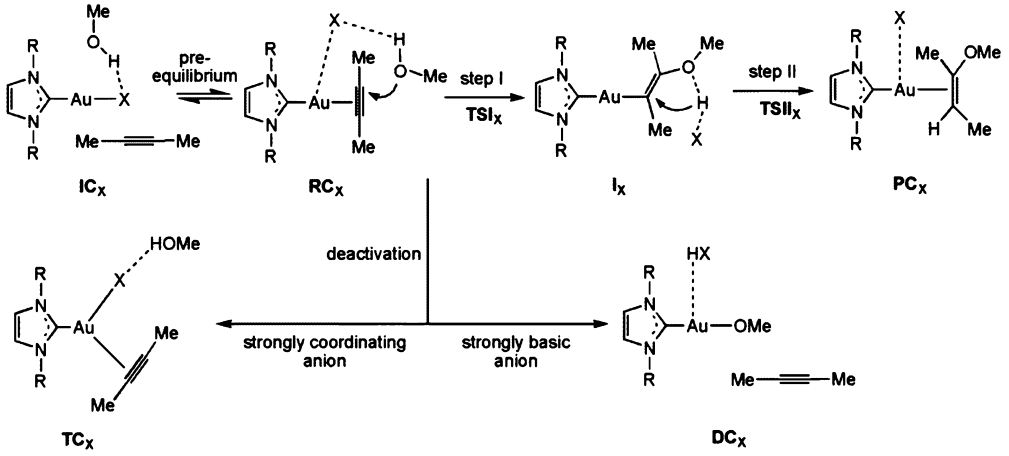

[a]The two steps, following the pre-equilibrium, are (I) nucleophilic attack of methanol to butyne via anion X^{-} template effect and activation of methanol by anion X^{-} proton acceptor properties and (II) proton transfer to substrate mediated by the anion X^{-} acting as a proton shuttle. Two catalyst deactivation pathways for strongly coordinating or strong basic anions are shown, leading to two alternative inactivated complexes.

Scheme 3. Schematic Representation of All the Species Considered in Our DFT Studied Reaction

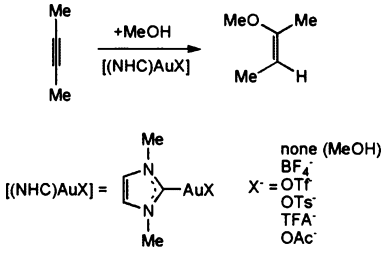

RESULTS AND DISCUSSION

Pre-equilibrium Step: Substrate vs Anion Coordination. We start our study with the searching for the most stable species formed by the catalyst, the anion and the nucleophile. Basicity and coordinating ability of the anion are investigated in the presence of methanol by examining the relative stabilities of the possible ternary adducts in the absence of 2-butyne substrate and, for comparison, the adduct without the anion but including an additional methanol molecule is considered. The inclusion of methanol allows to compare jointly both proton acceptor and coordinating ability of the different anions. To analyze the role of the methanol−anion interaction, we calculated the energy difference (in gas phase) between methanol-coordinated [NHCAu-($OHCH_3$)]X and anion-coordinated [NHCAu-X](CH_3OH) adducts. The optimized geometries of all the involved species are provided in the Supporting Information (SI), Figure S1, whereas the most stable adduct for each species is depicted in Figure 2.

In Table 1, the relative energies of the anion-coordinated [NHCAu-X](CH_3OH) and methanol-coordinated [NHCAu-($OHCH_3$)]X species are reported, and H−OCH_3 and X−$HOCH_3$ distances are summarized for the CH_3OH-coordinated species.

Indeed, the analysis of the ternary adducts of the $[NHC\text{-}Au]^+$ catalyst with X^- and methanol allows to probe the extent of the anion hydrogen-bonding ability. The distance between the anion and the hydrogen of the gold-coordinated methanol is

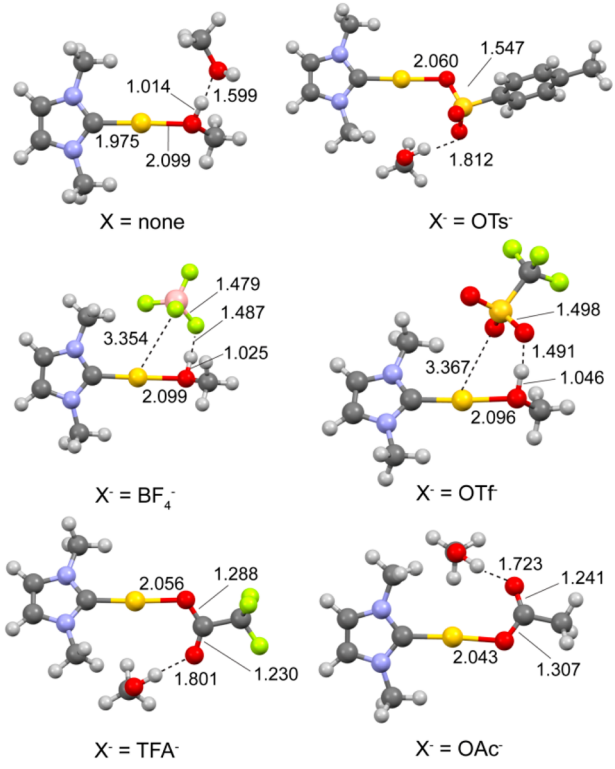

Figure 2. Optimized geometries of the most stable ternary adduct species. Distances are in angstroms.

1.062 Å for OAc^-, 1.255 Å for TFA^-, 1.425 Å for OTs^-, 1.487 Å for BF_4^-, and 1.491 Å for OTf^- (Table 1 and Figure 2).

The extent of proton transfer from gold-coordinated methanol to the anion correlates with the relative stability of the [NHCAu-($OHCH_3$)]X with respect to the [NHCAu-X](CH_3OH) adducts. Interestingly enough, for BF_4^- anion, the HB with gold-coordinated methanol does not tend to abstract the proton, rather it causes a B−F bond elongation from 1.404 to 1.479 Å (see Figure S1). For this reason, the distance between the hydrogen and the oxygen of the gold-coordinated methanol is a more suitable geometrical parameter to quantify

DOI: 10.1021/cs501681f
ACS Catal. 2015, 5, 803−814

Table 1. Relative Dissociation Energies (kcal/mol) Calculated As the Energy Difference between Methanol-Coordinated [NHCAu-($OHCH_3$)]X and Anion-Coordinated [NHCAu-X](CH_3OH) Species, Methanol O···H, and Anion−Methanol (CH_3OH···X) HB Distances (Å) in [NHCAu-($OHCH_3$)]X Species[a]

X^-	ΔE	CH_3O···H	CH_3OH···X
none (CH_3OH)	−34.4	1.014	1.599
OTs^-	+3.6	1.071	1.425
BF_4^-	−8.3	1.025	1.487
OTf^-	−0.5	1.046	1.491
TFA^-	+5.9	1.177	1.255
OAc^-	+5.7	1.468	1.062

[a]Species without anion and with one additional methanol are also shown.

the hydrogen-bonding basicity and, then, the nucleophilic activation ability of the different anions: the CH_3O···H distance is 1.468 Å for OAc^-, 1.177 Å for TFA^-, 1.071 Å for OTs^-, 1.046 Å for OTf^-, 1.025 Å for BF_4^-, and 1.014 Å for CH_3OH.

It can be seen that the [NHCAu-($OHCH_3$)]$^+$(CH_3OH) bond dissociation is calculated to be 34.4 kcal/mol with respect to [NHCAu(CH_3OH)$_2$]$^+$, where the two hydrogen-bonded methanol molecules form an additional HB with the backbone of the NHC ligand (Figure S1). In the presence of the anion, calculations predict that gold-anion bond adducts [NHCAu-X](CH_3OH) are more stable than gold−methanol bond adducts [NHCAu-($OHCH_3$)]X for all X^-, except for BF_4^- (−8.3 kcal/mol) and OTf^- (−0.5 kcal/mol). Notable, for OTs^-, ΔE is smaller than that for TFA^- or OAc^-.

Such a trend well correlates with the anion coordination power, identified with the metal−anion dissociation energies in a noncoordinating solvent (dichloroethane) and calculated by Lledós et al.[11b] for [PAuX] → [PAu]$^+$ + X^- (P = PH_3 and PPh_3, X^- = TFA^-, Cl^-, NO_3^-, OTs^-, OTf^-, and BF_4^-). However, our calculated ΔE values in Table 1 are generally lower than those computed by Lledós et al., and this is due to the presence of a CH_3OH···X HB, which facilitates the decoordination of the anion. If the anion is a strong base, experimental observations showed that the alcoholic proton is completely abstracted from the methanol, with the formation of a methoxide moiety.[14]

The first step of the catalysis is the ligand substitution, CH_3OH or X^-, by the alkyne. Quaternary adducts formed between the anion X^-, methanol, 2-butyne, and [NHC-Au]$^+$ were computationally found in which the 2-butyne is coordinated through its triple bond. However, the initial complex ($\mathbf{IC_X}$) is represented by the most stable ternary adduct calculated above for each anion plus the 2-butyne substrate in the second coordination sphere (see Scheme 2).

Coordination of 2-butyne to the metal center leads to different conformations. Among them, two conformations are of interest for the nucleophilic attack step. In the most stable one, the hydrogen-bonded [$X(CH_3OH)$]$^-$ group is located above the gold. We denote it as structure $\mathbf{NC_X}$ (**n**onactivating **c**omplex), and it is given in the SI for all the species (Figures S2 and S3).

The $\mathbf{NC_X}$ conformation corresponds either to the reactant complex for the nucleophilic attack in the syn periplanar (inner-sphere) mechanism, which is unfavorable on the basis of the calculations (it was not possible to locate a transition state for this mechanism on the potential energy surface) and on experimental grounds,[13] or to a nonactivating complex for the nucleophilic attack in the outer-sphere mechanism.

In the second conformation, the [$X(CH_3OH)$]$^-$ group occupies an area around the alkyne but in the opposite site of the Au center and its energy is generally slightly higher than that of $\mathbf{NC_X}$. It represents the reactants complex for the nucleophilic attack to the C−C triple bond in the anti periplanar (outer-sphere) mechanism (structure $\mathbf{RC_X}$ in Scheme 2).

The optimized geometries of the initial complexes $\mathbf{IC_X}$, the reactant complexes for the outer-sphere mechanism $\mathbf{RC_X}$, and the tricoordinated $\mathbf{TC_X}$ complexes are shown in Figure 3 for X = none (CH_3OH), OTs^-, BF_4^-, OTf^-, TFA^-, and OAc^-, where the relative stabilities of the $\mathbf{RC_X}$ and $\mathbf{TC_X}$, calculated with respect to the $\mathbf{IC_X}$, are also reported.

First we consider the catalyst without the anion. The alkyne catalytic cycle initiates when the 2-butyne passes from the second ($\mathbf{IC_{none}}$) to the first coordination sphere. The optimized structures after ligand substitution can be described as linear gold complexes, where the two Au−C bond distances are slightly different in $\mathbf{RC_{none}}$ (2.206 and 2.234 Å). The consequence of the alkyne coordination is the lengthening of the triple bond (the C−C distance is 1.216 Å in $\mathbf{IC_{none}}$ and 1.243 Å when coordinated). The $(CH_3OH)_2$ dimer forms a weak interaction with a hydrogen of the butyne through (CH···O−H = 2.069 Å) in $\mathbf{RC_{none}}$. Optimization of a tricoordinated structure, where both the butyne and one methanol molecule are coordinated to gold, was unsuccessful, always ending up in two-coordinated structures as $\mathbf{NC_{none}}$ and $\mathbf{RC_{none}}$. The former is more stable than the initial complex by 1.4 kcal/mol, whereas the latter is less stable by 1.2 kcal/mol (Figure S2 and Figure 3).

Now we consider the inclusion of the anion X^-. The initial quaternary complex $\mathbf{IC_X}$ is the anion-coordinated species with the 2-butyne in the second coordination sphere, [NHCAu-X](CH_3OH)(2-butyne), except for BF_4^- and OTf^-, for which the methanol-coordinated species is more stable and is taken as the initial complex. For BF_4^- and OTs^- $\mathbf{IC_X}$s the 2-butyne is weakly interacting through HB with the NHC ligand, whereas for OTf^-, TFA^-, and OAc^- it forms an HB with the oxygen atom of the methanol or the anion coordinated to Au (Figure 3).

After ligand substitution, in the butyne-coordinated complexes the [$(CH_3OH)X$]$^-$ adduct can be found either at the same side of the substrate ($\mathbf{RC_X}$) or between the catalyst and the substrate, weakly or strongly interacting with the Au center through the X^- anion (see $\mathbf{NC_X}$ structures in Figures S2 and S3).

In all $\mathbf{RC_X}$ complexes at least one basic atom of the anion weakly interacts with the metal center (Au···O = 3.283 Å for OTs^-, 3.332 Å for OTf^-, 3.105 Å for TFA^-, and 2.907 Å for OAc^-; Au···F = 3.204 Å for BF_4^-, Figure 3) while forming an HB with methanol. The oxygen atom of methanol is at about 3.1−3.2 Å distance from the closest carbon atom of the coordinated butyne.

The search for tricoordinated species, either having the 2-butyne and the anion ($\mathbf{TC_X}$) (see Scheme 2 and Figure 3) or the 2-butyne and the methanol ($\mathbf{TC_{Nuc}}$) (Figure S3) coordinated to the metal, was successful for TFA^- and OAc^- but not for OTs^-, BF_4^-, and OTf^-, always ending up in two-coordinated structures. Tricoordinated species $\mathbf{TC_X}$ thus represent substitution reaction intermediates for TFA^- and OAc^-, whereas $\mathbf{TC_X}$ is a transition state for OTs^- (see below).

DOI: 10.1021/cs501681f
ACS Catal. 2015, 5, 803−814

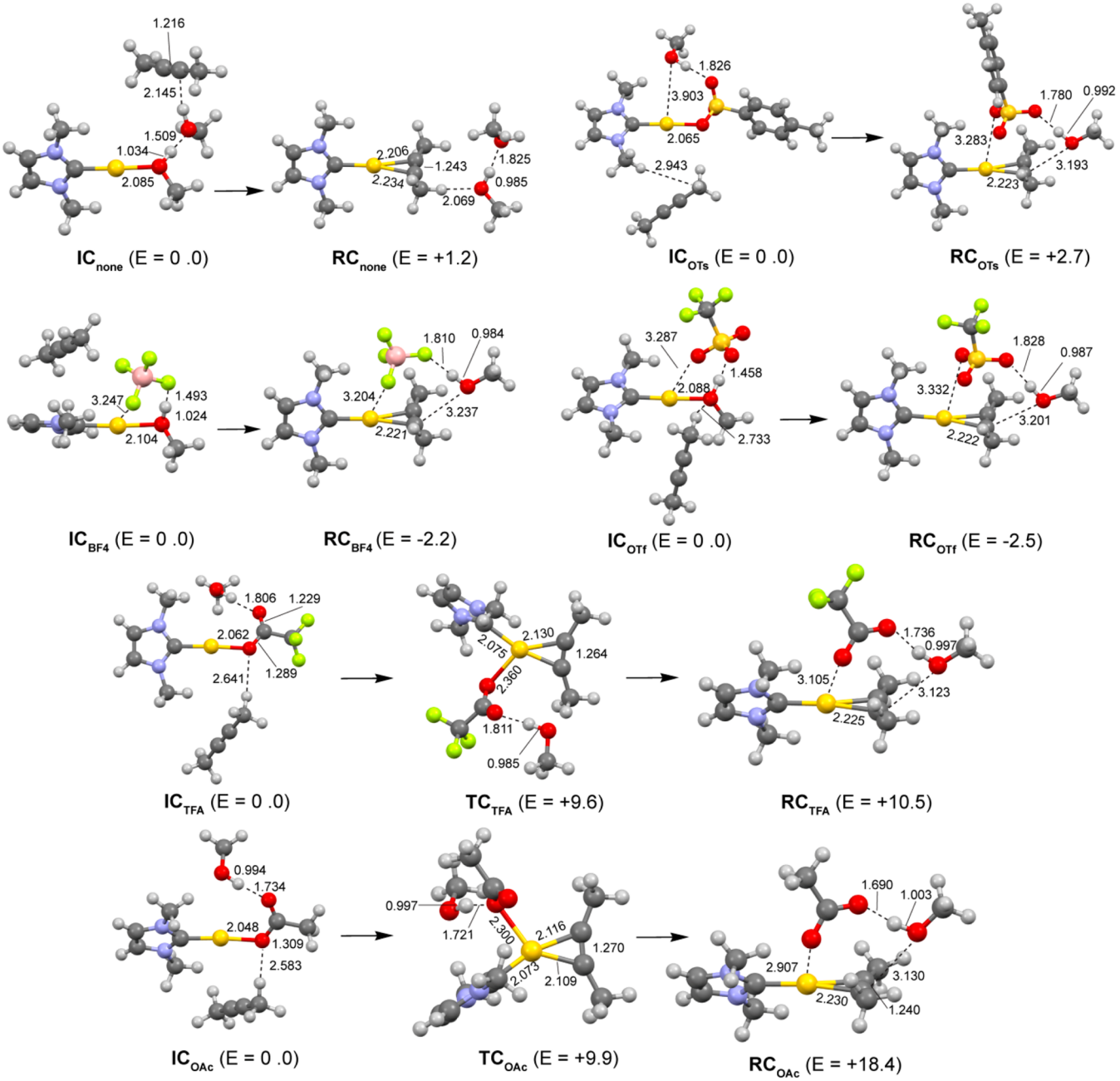

Figure 3. Optimized geometries of the initial complex $\mathbf{IC_X}$, reactants complex for outer-sphere attack $\mathbf{RC_X}$ and intermediate tricoordinated complex $\mathbf{TC_X}$ for all the considered quaternary adducts. Distances are in angstroms. Relative stabilities of $\mathbf{RC_X}$ and $\mathbf{TC_X}$ with respect to $\mathbf{IC_X}$ are also reported (kcal/mol).

In $\mathbf{TC_{TFA}}$, TFA^- forms relatively strong interaction with the gold center through one of its oxygen atoms (Au···O = 2.360 Å), also strengthening the 2-butyne/gold interaction (Au···C = 2.130 and 2.127 Å, compared to 2.22 Å in the two-coordinated complexes and C−C = 1.264 Å compared to 1.24 Å in two-coordinated complexes) (Figure 3). The OAc^- anion forms even stronger interaction with the metal in $\mathbf{TC_{OAc}}$, with an Au−O distance of 2.300 Å, also in this case with a strengthening of the 2-butyne/gold interaction (Au···C = 2.109 and 2.116 Å, C−C = 1.270 Å) (Figure 3).

Very interestingly, in the two-coordinated $\mathbf{RC_{OAc}}$, the nucleophile locates near the 2-butyne, forming one HB between the oxygen atom of the anion and the proton of the methanol (O···H = 1.690 Å, CH_3O−H = 1.003 Å), thus revealing again a strong proton acceptor behavior of OAc^-.

All the $\mathbf{NC_X}$ complexes are slightly more stable than the reactant complexes $\mathbf{RC_X}$ for OTs^-, BF_4^-, OTf^-, and TFA^- (in the range 0.9−2.9 kcal/mol). For TFA^- the tricoordinated complex $\mathbf{TC_{TFA}}$ is 1.8 kcal/mol less stable than $\mathbf{NC_{TFA}}$ and only 0.9 kcal/mol more stable than $\mathbf{RC_{TFA}}$. The exception is OAc^-: the tricoordinated complex $\mathbf{TC_{OAc}}$ is calculated to be the most stable structure, 8.5 kcal/mol more stable than $\mathbf{RC_{OAc}}$.

The formation of the $\mathbf{RC_X}$ adducts from the corresponding initial complexes $\mathbf{IC_X}$ is thermodynamically favored for BF_4^- and OTf^-, with energies of −2.2 and −2.5 kcal/mol, respectively. For OTs^-, TFA^-, and OAc^- the reaction is endothermic by +2.7, +10.5, and +18.4, respectively, but the

DOI: 10.1021/cs501681f
ACS Catal. 2015, 5, 803−814

RC_X adduct is easily accessible from NC_X for OTs^- (0.9 kcal/mol) and TFA^- (2.7 kcal/mol) (Table 2). The thermodynamical analysis shows that, at least for OAc^-, the anion substitution by substrate process is not feasible. The RC_{OAc} is less favorable than IC_{OAc} by 18.4 kcal/mol, meaning that the $IC_{OAc} \rightarrow RC_{OAc}$ equilibrium should be shifted toward IC_{OAc} and the activation barrier for the OAc^- substitution is certainly larger than 18.4 kcal/mol, that looks already quite high.

Table 2. Relative IC_X and RC_X Energies (kcal/mol), Metal−Anion (M···X) (the Anion Basic Atom Closest to the Metal Is Reported) and Metal−Hydrogen (M···$HOCH_3$) Bond Distances (Å) in RC_X[a]

X^-	ΔE	M···X	X···$HOCH_3$
none-CH_3OH	+1.2		1.825
OTs^-	+2.7	3.283	1.780
BF_4^-	−2.2	3.204	1.810
OTf^-	−2.5	3.332	1.828
TFA^-	+10.5	3.105	1.736
OAc^-	+18.4	2.907	1.690

[a]Species without anion with one additional CH_3OH are also shown.

Thus, the RC_X formation energy *in the presence of methanol* is in the order $OAc^- > TFA^- > OTs^- > BF_4^- > OTf^-$ (see Table 2). However, this trend is a result of a net balance between the metal coordinating and the proton acceptor abilities of the anion. Indeed, in our preliminary calculations for OTs^-,[14] we already noticed that in the absence of methanol, the NC_{OTs} formation energy from IC_{OTs} is +3.6 kcal/mol, indicating a somewhat unfavorable alkyne substitution of the coordinated OTs^-, whereas this value lowers to +1.8 kcal/mol when one molecule of methanol is introduced, thanks to the HB formation between the methanol and the anion. However, whether the OTs^- substitution process is feasible or not could be crucial for explaining the best catalytic efficiency by OTs^-. For this counterion the energy barrier for the reaction $IC_{OTs} \rightarrow NC_{OTs}$ has been calculated to be 11.5 kcal/mol, and the transition state structure, a tricoordinated species, is shown in Figure S4 (TS_Preeq_{OTs}). This result indicates a feasible anion substitution by alkyne.

This picture is consistent with the experimental results where no catalytic activity was found using OAc^- as anion. The high coordination energy of OAc^- makes the formation of the reactant complex RC_{OAc} highly disfavored. On the other hand, one could be tempted to predict that the most active anion should be OTf^-, since for the latter the RC_{OTf} is the most stable one. Unfortunately, pre-equilibrium alone, mostly driven by the coordinating ability of the anion, cannot explain the experimentally observed trend, according to which the catalytic activity is higher when OTs^- is used.

In the next section the addition of methanol to 2-butyne will be investigated in detail.

Nucleophilic Attack (Step I) and Protodeauration (Step II). The reactant complex RC_X, where the anion acts as a template, holding the reactive methanol molecule in the right position for an outer-sphere addition, will be the starting complex for the study of this process.

First we analyze the cationic butyne-coordinated species, $[NHCAu\text{-}(2\text{-butyne})]^+(CH_3OH)_2$ $RC_{none\text{-}MeOH}$, in the absence of the anion. The inclusion of a second methanol molecule is needed to activate the first methanol molecule (nucleophile), which otherwise would be not sufficiently nucleophilic to attack the substrate. All our attempts to locate a transition state for the nucleophilic attack without the anion and only one molecule of methanol failed.

The activation barrier corresponding to the transition state structure involved in the outer-sphere nucleophilic attack amounts to 12.0 kcal/mol (Figure 4). The transition state ($TSI_{none\text{-}MeOH}$) evolves with the formation of the intermediate $I_{none\text{-}MeOH}$, which is less stable than $RC_{none\text{-}MeOH}$ by 8.9 kcal/mol (3.1 kcal/mol more stable than the transition state leading to it, Figure 4). In $TSI_{none\text{-}MeOH}$, the bond between the gold center and the carbon atom on which the nucleophile attacks (C1) is elongated (2.770 Å), while that between the gold and the other carbon of the triple bond (C2) becomes shortened (2.100 Å).

Simultaneously, the C1−C2 bond length increases (1.283 Å) and the distance between C1 and the oxygen atom of the nucleophile is 1.988 Å. The intermediate $I_{none\text{-}MeOH}$ structure is very similar to that of the transition state, with a much reduced C1···O distance (1.565 Å). The second methanol molecule assisting the nucleophilic attack is not sufficiently strong to

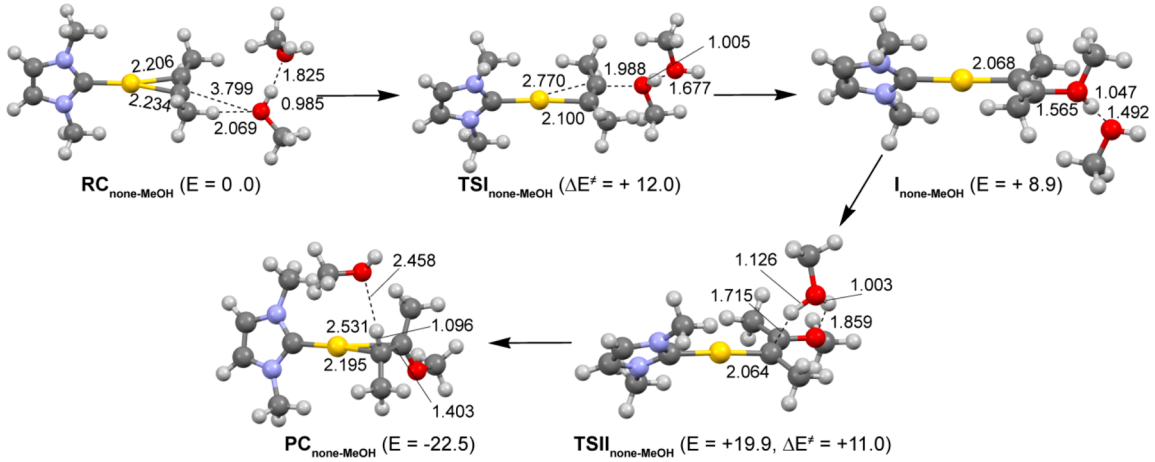

Figure 4. Reactant complex $RC_{none\text{-}MeOH}$, intermediate $I_{none\text{-}MeOH}$, product complex $PC_{none\text{-}MeOH}$, transition state $TSI_{none\text{-}MeOH}$ for the methanol nucleophilic attack (step I), and transition state $TSII_{none\text{-}MeOH}$ for the proton migration (step II) for the addition of methanol to 2-butyne reaction in the absence of the anion. Energies values (kcal/mol) refer to $RC_{none\text{-}MeOH}$ taken as zero. Bond lengths are in angstroms.

DOI: 10.1021/cs501681f
ACS Catal. 2015, 5, 803−814

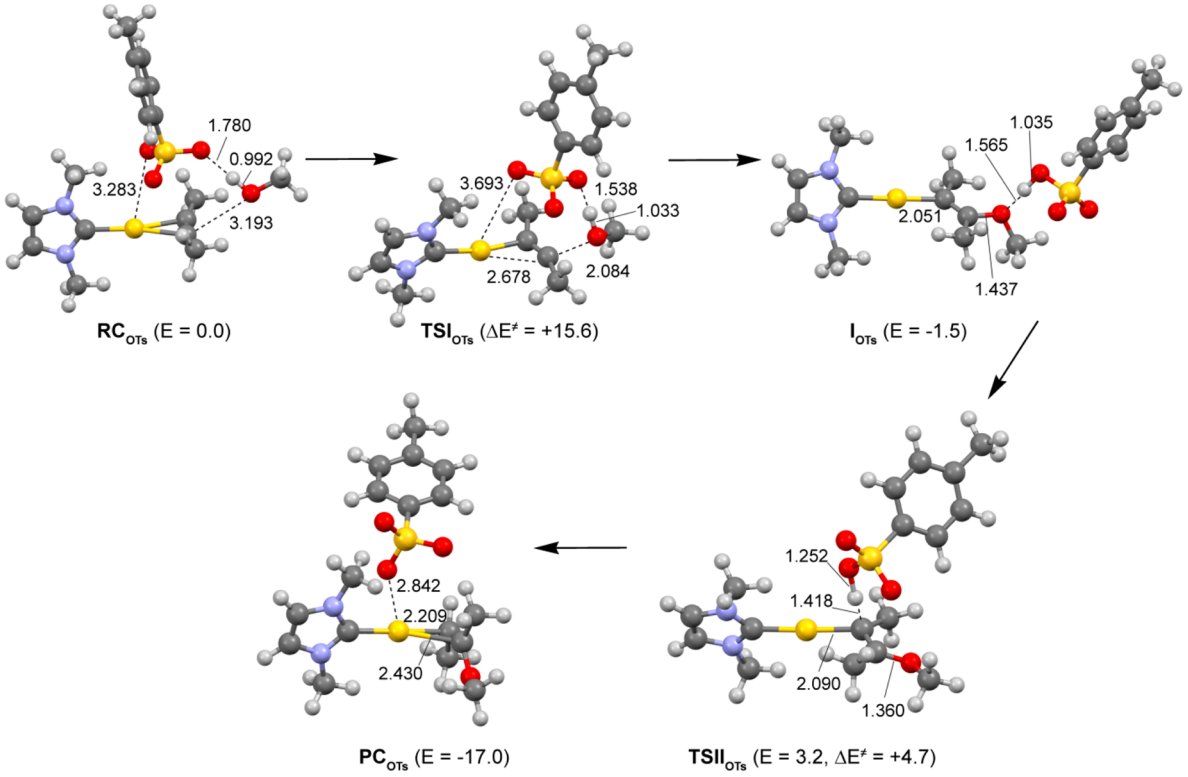

Figure 5. Reactants complex $\mathbf{RC}_{OTs}$, intermediate $\mathbf{I}_{OTs}$, product complex $\mathbf{PC}_{OTs}$, transition state $\mathbf{TSI}_{OTs}$ for the methanol nucleophilic attack (step I), and transition state $\mathbf{TSII}_{OTs}$ for the proton migration (step II) for the addition of methanol to butyne reaction in the presence of the OTs^- anion. Energies values (kcal/mol) refer to $\mathbf{RC}_{OTs}$ taken as zero. Bond lengths are in angstroms.

abstract the proton from the coordinated nucleophile: the O−H bond length in coordinated methanol is 1.047 Å, and the hydrogen of the coordinated methanol is at a distance of 1.492 Å from the O atom of the assisting methanol molecule.

The methanol addition is completed by the migration of the proton bound to the oxygen atom of the nucleophile in the intermediate complex $\mathbf{I}_{\text{none-MeOH}}$ to C2 (protodeauration), through the transition state $\mathbf{TSII}_{\text{none-MeOH}}$. In the latter, the second molecule of methanol acts simultaneously as a proton acceptor (with respect to the coordinated methanol, O···H1 = 1.003 Å), and a proton donor (with respect to C2, O···H2 = 1.126 Å). The calculated activation barrier for this step is 11.0 kcal/mol, and the product is highly stabilized with respect to the intermediate species (−31.4 kcal/mol). $\mathbf{TSII}_{\text{none-MeOH}}$ evolves to the final product complex ($\mathbf{PC}_{\text{none-MeOH}}$, Figure 4), in which the organic moiety is η^2-coordinated to the gold via its remaining unsaturated double bond in an asymmetric fashion (Au···C2 = 2.195, Au···C1 = 2.531 Å). The ΔE for the overall reaction of methanol addition to 2-butyne is calculated to be exothermic by −22.5 kcal/mol. From the whole reaction energy profile, it is evident that the hydrogen atom migration is subjected to only a slightly lower energy barrier than the initial nucleophile attack step (11.0 vs 12.0 kcal/mol, Figure 4), but it is important to note that the absolute energy of $\mathbf{TSII}_{\text{none-MeOH}}$ is higher than that of $\mathbf{TSI}_{\text{none-MeOH}}$ (19.9 vs. 12.0 kcal/mol with respect to the $\mathbf{RC}_{\text{none-MeOH}}$, respectively).

Next, we consider only three out of the five different anions X^-, namely OTs^-, BF_4^-, and OAc^-, as representative for the activity observed experimentally, in order to emphasize the critical role of the anion. In particular, OTs^- and BF_4^- have been chosen because the former shows a higher catalytic activity than the latter, in spite of its higher coordinating ability, while OAc^- has been chosen for its catalyst deactivator behavior. The concerted nucleophilic attack to butyne and hydrogen abstraction from nucleophile by the anion (i.e., nucleophile activation) has been investigated with the aid of two-dimensional plots of the energy, which are provided in the Supporting Information with relative computational details (Figures S5 and S6). For BF_4^-, two additional two-dimensional energy plots have been constructed for concerted nucleophilic attack/protodeauration mechanism and for protodeauration step with an additional methanol molecule and they are also presented in the Supporting Information (Figures S7 and S8).

Let us focus on OTs^- first.

The transition state for the nucleophilic attack step gives an activation barrier of 15.6 kcal/mol and the formation of the intermediate ($\mathbf{I}_{OTs}$) is exothermic by 1.5 kcal/mol (Figure 5).

In the $\mathbf{TSI}_{OTs}$ the attack of methanol at C1 causes gold to change its coordination, forming an almost direct bond with the other carbon atom that lies at 2.101 Å from it. The C1−C2 bond length increases (1.275 Å), and the distance between C1 and the oxygen atom of the nucleophile is 2.084 Å. An incipient abstraction of hydrogen of methanol by OTs^- can be observed (CH_3O−H = 1.033 Å, CH_3OH···O(OTs^-) = 1.538 Å). Very interestingly, the characteristic template structure of $\mathbf{RC}_{OTs}$ with the anion in a bridging position between Au and methanol is retained in $\mathbf{TSI}_{OTs}$.[14]

In the intermediate complex $\mathbf{I}_{OTs}$ the H−O(OTs) distance is 1.035 Å and the CH_3O···H is 1.565 Å, therefore the hydrogen of methanol has been completely abstracted by OTs^-, and this causes a larger stabilization of the intermediate $\mathbf{I}_{OTs}$ (−1.5 kcal/mol) with respect to the corresponding species formed with the additional methanol molecule, in the absence of the anion (+8.9 kcal/mol).

DOI: 10.1021/cs501681f
ACS Catal. 2015, 5, 803−814

For the protodeauration, the fact that anions can assist and facilitate proton transfers by lowering the energy barriers is well-known in literature.[11b,22] In the transition state $\mathbf{TSII}_{\mathbf{OTs}}$ the proton is found between the OTs^- oxygen (H···O = 1.252 Å) and C2 (H···C2 = 1.418 Å), therefore the proton transfer takes place in one step. In the product complex $\mathbf{PC}_{\mathbf{OTs}}$, the hydrogen is bound to C2 in the trans position with respect to the methoxy and the product is η^2-coordinated to the gold via its remaining unsaturated double bond (Au···C2 = 2.209, Au···C1 = 2.430 Å), with the OTs^- weakly interacting with the gold center.

The calculated energy barrier for the hydrogen transfer to the carbon is only 4.7 kcal/mol. The product complex $\mathbf{PC}_{\mathbf{OTs}}$ is stabilized with respect to the intermediate $\mathbf{I}_{\mathbf{OTs}}$ by 15.5 kcal/mol, and the ΔE for the overall reaction of methanol addition to 2-butyne is −17.0 kcal/mol (Figure 5).

To check the effect of an additional nucleophile molecule mediating the proton transfer on the activation barriers, the nucleophilic attack and protodeauration steps have been recalculated for OTs^- with the inclusion of a second methanol molecule. The reactants complex $\mathbf{RC}_{\mathbf{OTs\text{-}MeOH}}$, intermediate $\mathbf{I}_{\mathbf{OTs\text{-}MeOH}}$, product complex $\mathbf{PC}_{\mathbf{OTs\text{-}MeOH}}$, transition state $\mathbf{TSI}_{\mathbf{OTs\text{-}MeOH}}$, and transition state $\mathbf{TSII}_{\mathbf{OTs\text{-}MeOH}}$ structures and energies referred to $\mathbf{RC}_{\mathbf{OTs\text{-}MeOH}}$ taken as zero are provided in Figure S9. Indeed, the activation barrier of the step I is greatly lowered to 7.3 kcal/mol (compared to 15.6 kcal/mol including only one methanol molecule), whereas the activation barrier for step II is not affected (4.7 kcal/mol, the same value as in the case with only one methanol molecule).

We move now to BF_4^- anion assisted nucleophilic attack of methanol to butyne.

Also in this case the formation of the O−C1 bond (nucleophilic attack to butyne) and the H−F bond formation (hydrogen abstraction from nucleophile by anion) is a concerted process, although in the intermediate $\mathbf{I}_{\mathbf{BF4}}$ the optimal H···F distance is at about 1.25 Å and the hydrogen abstraction is not complete. A transition state calculation shows that the activation energy required for $\mathbf{TSI}_{\mathbf{BF4}}$ is 16.5 kcal/mol and the formed intermediate $\mathbf{I}_{\mathbf{BF4}}$ is 9.9 kcal/mol above the reactants complex $\mathbf{RC}_{\mathbf{BF4}}$ (Figure 6). In $\mathbf{TSI}_{\mathbf{BF4}}$ the distance between the oxygen atom of methanol and C1 is 1.994 Å, and, simultaneously, gold changes its coordination, forming an almost direct bond with C2 that lies 2.092 Å from it, and the C1−C2 bond distance increases to 1.282 Å. An incipient abstraction of hydrogen of methanol by BF_4^- can also be observed (CH_3O−H = 1.014 Å, $CH_3OH\cdots FBF_3^-$ = 1.550 Å), but less pronounced than that by OTs^-. Similarly to OTs^-, the characteristic template structure of $\mathbf{RC}_{\mathbf{BF4}}$ with the anion in a bridging position between Au and methanol is retained in $\mathbf{TSI}_{\mathbf{BF4}}$.

In the intermediate structure $\mathbf{I}_{\mathbf{BF4}}$ the methanol nucleophile hydrogen atom has not been completely abstracted by the BF_4^- anion. However, quite interestingly, the H−F distance is 1.278 Å and the B−F bond length elongates to 1.556 Å.

Compared to the intermediate species with the OTs^- anion, BF_4^-, although less coordinating, is a less effective hydrogen acceptor from methanol than OTs^-, and the activation barrier for the nucleophilic attack is slightly higher (16.5 vs 15.6 kcal/mol), in agreement with the experiment.[14]

For the proton transfer step, in an attempt to find a transition state structure by approaching the methanol proton to C1, a very high energy structure, characterized by a four-membered COHC-ring, has been found.

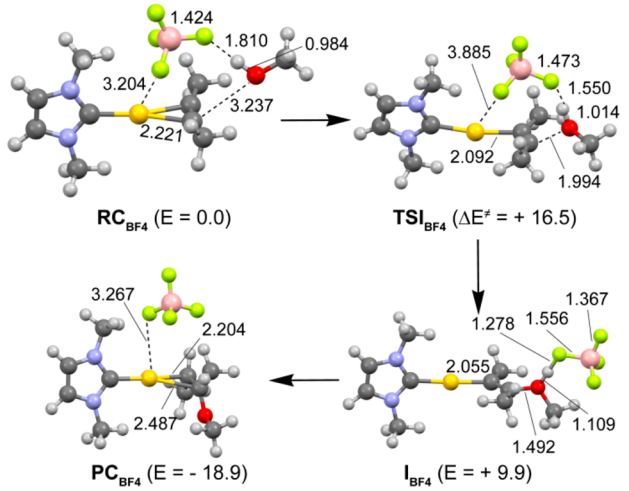

Figure 6. Reactant complex $\mathbf{RC}_{\mathbf{BF4}}$, intermediate $\mathbf{I}_{\mathbf{BF4}}$, product complex $\mathbf{PC}_{\mathbf{BF4}}$, and transition state $\mathbf{TSI}_{\mathbf{BF4}}$ for the methanol nucleophilic attack (step I) for the addition of methanol to 2-butyne reaction in the presence of BF_4^-. Energy values (kcal/mol) refer to $\mathbf{RC}_{\mathbf{BF4}}$ taken as zero. Bond lengths are in angstroms.

An estimate of the energy barrier for this process would lead to a very high value, higher than 40 kcal/mol (at BP86 level). This barrier would be too high, thus this pathway can be ruled out and two alternatives pathways, one considering a concerted nucleophilic attack to butyne and proton migration to the second carbon atom and one including a second methanol molecule mediating the proton transfer, have been considered (see two-dimensional energy plots, Figures S7 and S8, respectively).

Due to the calculated very high activation energy (larger than 40 kcal/mol al BP86 level, see Figure S7), also the concerted nucleophilic attack/proton migration process can be ruled out too.

On the other hand, inclusion of a second methanol molecule has indeed a beneficial effect on the whole step. The activation barrier of the step I drops to 14.8 kcal/mol and the endothermicity to 6.4 kcal/mol (Figure 7).

In $\mathbf{RC}_{\mathbf{BF4\text{-}MeOH}}$, BF_4^- and the additional CH_3OH molecules bridge the Au center and the attacking methanol, building up a chain. The anion distance from Au decreases to 3.133 Å and the anion···$HOCH_3$ distance is 1.736 Å. Compared to $\mathbf{TSI}_{\mathbf{BF4}}$ for the process with only one methanol molecule, the $\mathbf{TSI}_{\mathbf{BF4\text{-}MeOH}}$ including two methanol molecules shows that the nucleophilicity of the attacking methanol molecule is enhanced by the $BF_4^-\cdots HOCH_3$ chain, acting as a better proton acceptor than the single BF_4^-: the distance between the oxygen atom of the nucleophile and C1 is 2.035 Å, and an incipient abstraction of hydrogen of methanol nucleophile by additional CH_3OH is observed (CH_3O−H = 1.029 Å), as well as of hydrogen of additional methanol by BF_4^- (CH_3O−H = 1.000 Å).

In the intermediate structure $\mathbf{I}_{\mathbf{BF4\text{-}MeOH}}$, the methanol nucleophile hydrogen atom has been almost completely abstracted by the additional CH_3OH (CH_3O−H = 1.378 Å), which acts both as a proton acceptor and a proton donor (CH_3O−H = 1.090 Å with the proton from nucleophile, CH_3O−H = 1.067 Å with the proton interacting with BF_4^-).

As also noticed in literature, the solvent molecules play a central role in the overall reaction mechanism, since the participation of other molecules (like the additional methanol molecule) can lead to significantly lower reaction barriers and

DOI: 10.1021/cs501681f
ACS Catal. 2015, 5, 803−814

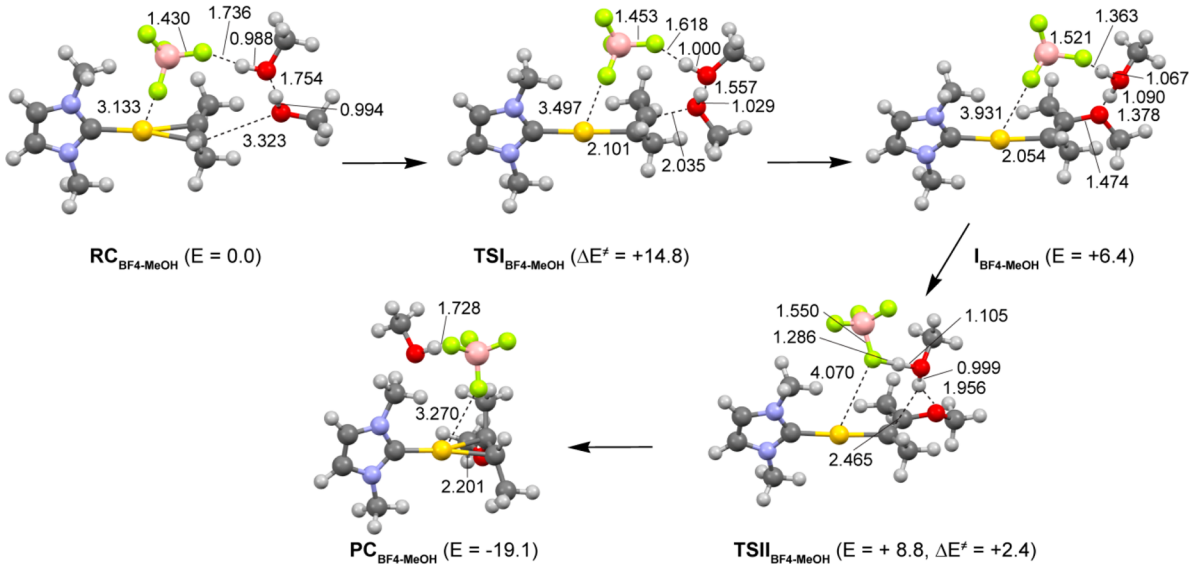

Figure 7. Reactant complex $\mathbf{RC}_{\mathbf{BF4\text{-}MeOH}}$, intermediate $\mathbf{I}_{\mathbf{BF4\text{-}MeOH}}$, product complex $\mathbf{PC}_{\mathbf{BF4\text{-}MeOH}}$, transition state $\mathbf{TSI}_{\mathbf{BF4\text{-}MeOH}}$ for the methanol nucleophilic attack (step I), and transition state $\mathbf{TSII}_{\mathbf{BF4\text{-}MeOH}}$ for the proton migration (step II) for the addition of methanol to 2-butyne reaction in the presence of the BF_4^- anion with an additional methanol molecule. Energy values (kcal/mol) refer to $\mathbf{RC}_{\mathbf{BF4\text{-}MeOH}}$ taken as zero. Bond lengths are in angstoms.

to a much more efficient proton transfer than in the strictly molecular case.[5b,e]

In the intermediate product $\mathbf{I}_{\mathbf{BF4\text{-}MeOH}}$, the methanol-coordinated hydrogen has been almost completely transferred to the additional methanol (H−O = 1.090 Å) which is forming an HB with the anion. In the transition state $\mathbf{TSII}_{\mathbf{BF4\text{-}MeOH}}$ the migrating proton is far from the methanol nucleophile oxygen (1.956 Å), bound to the additional methanol molecule (O−H = 0.999 Å) and at a distance of 2.465 Å from the unsaturated carbon atom, while BF_4^- is accepting the second proton from the additional methanol (F−H = 1.286 Å, O−H = 1.105 Å).

The actual proton transfer takes place in one step, where the additional methanol plays a crucial role. In the product complex $\mathbf{PC}_{\mathbf{BF4\text{-}MeOH}}$, the hydrogen is bound to carbon in the trans position with respect to methoxy and the product is coordinated to gold via its remaining unsaturated double bond in an asymmetric fashion (Au−C = 2.201, 2.474 Å), with the BF_4^- weakly interacting with the gold center.

The calculated energy barrier for the hydrogen transfer to the carbon is only 2.4 kcal/mol. This barrier is very low, thus showing that the proton transfer is greatly facilitated by the additional CH_3OH-BF_4^- proton shuttle chain.

The product complex $\mathbf{PC}_{\mathbf{BF4\text{-}MeOH}}$ is stabilized with respect to intermediate $\mathbf{I}_{\mathbf{BF4\text{-}MeOH}}$ by 25.5 kcal/mol, and the ΔE for the overall reaction of methanol addition to 2-butyne is −19.1 kcal/mol. Ultimately, with the inclusion of a second methanol molecule, the activation barrier for the nucleophilic attack is much higher in case of BF_4^- (14.8 kcal/mol) in comparison with OTs^- (7.3 kcal/mol).

In Figure 8, all the energy profiles for OTs^-, BF_4^-, including both one and two nucleophile molecules, and for the species without the counterion are summarized. From this figure it can be easily seen that inclusion of two methanol molecules is crucial to see the effect of each counterion on each step of the profile. In addition, the reaction mechanism with OTs^- and BF_4^- with two methanol molecules can be directly compared to that with the catalyst without the anion. We conclude that the anion greatly facilitates the proton migration step (activation

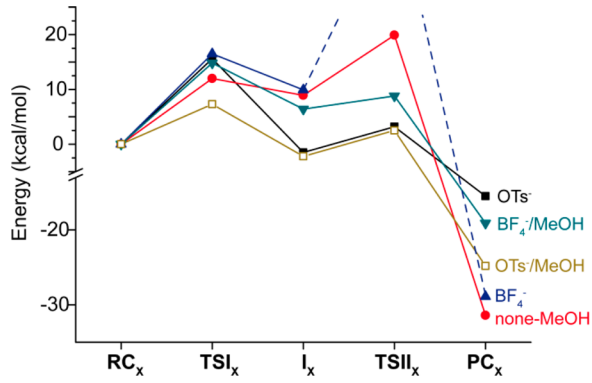

Figure 8. Energy profiles for the nucleophilic attack (step I) and protodeauration (step II) for OTs^-, BF_4^-, including one (OTs^-, BF_4^-) and two (OTs^-/MeOH, BF_4^-,/MeOH) methanol molecules, and without the anion (none-MeOH).

energy 2.4 kcal/mol for BF_4^- and 4.7 kcal/mol for OTs^- vs 11.0 kcal/mol without the anion, respectively), making the nucleophilic attack the rate-determining step. The nucleophilic attack is, in turn, greatly facilitated by a stronger proton acceptor anion.

Catalyst Deactivation Pathways. In order to analyze the catalyst deactivation pathways competing with the first nucleophilic attack step, we investigate a hypothetical OAc^- assisted nucleophilic attack of methanol to 2-butyne, with the aid of the two-dimensional plot of the energy, which is provided in the SI (Figure S10). The plot gives an interesting view of the catalyst inactivating process in the nucleophilic attack step and five key point structures are shown in Figure 9. A starting low energy point is represented by structure **A** (−3.9 kacl/mol with respect to $\mathbf{RC}_{\mathbf{OAc}}$) that is somewhat similar to $\mathbf{TC}_{\mathbf{OAc}}$, the most stable structure where both the butyne and the anion are coordinated to gold (compare Figures 3 and 9). A transition state can be reached easily by shortening the O−H distance to 1.2 Å, which represents the transition state for hydrogen abstraction from methanol. The geometry optimization with

DOI: 10.1021/cs501681f
ACS Catal. 2015, 5, 803−814

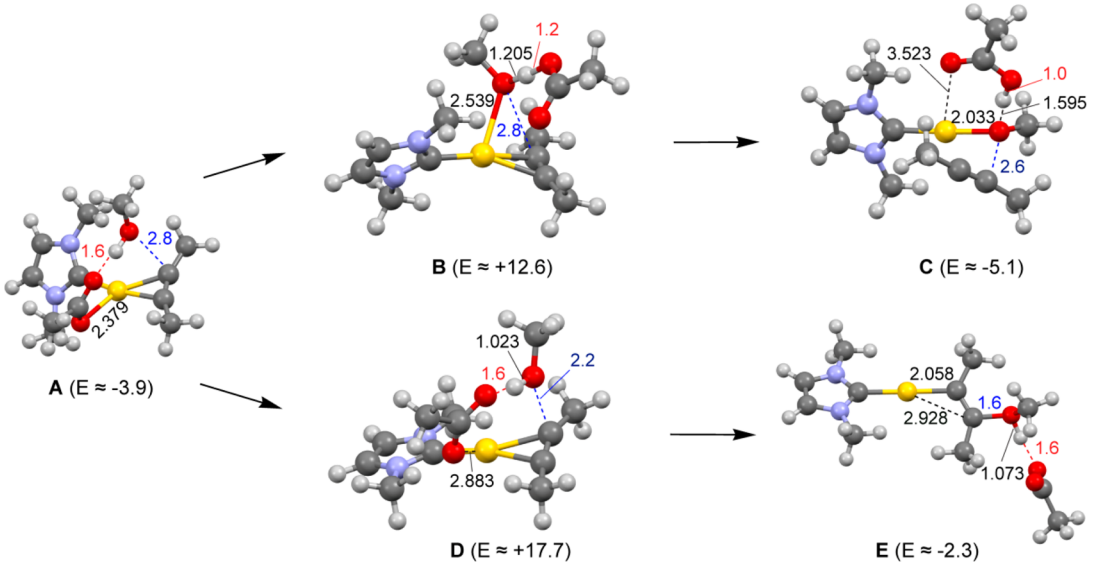

Figure 9. Optimized geometries at five key points in the two-dimensional contour plot (Figure S8) for the C−O bond formation and OAc^- proton abstraction pathways: low-energy structure (structure **A**); estimated transition state for proton abstraction (structure **B**); estimated product complex from proton abstraction path (structure **C**); estimated transition state for C−O bond formation (structure **D**); estimated product complex from C−O bond formation path (structure **E**). The fixed parameters are shown in red and blue. Estimated energy values at the DFT/BP86 level are in kilocalories per mole; distances are in angstroms (see text).

O−C1 fixed at 2.8 Å and O−H at 1.2 Å gives the structure shown in Figure 9, denoted as **B**. As we can see from Figure S10, the hydrogen abstraction by OAc^- takes place before the nucleophilc attack starts, since the O−C1 distance is still very large. Moreover, the hydrogen abstraction is able to induce the anion decoordination from gold. Then the system proceeds to a low-energy region (at about O−C1 = 2.5 Å and O−H = 1.0 Å). The geometry optimization with O−C1 fixed at 2.6 Å and O−H at 1.0 Å gives the structure **C** (Figure 9), which shows that the 2-butyne has been released and CH_3O^- methoxy species formed is coordinated to Au, with the protonated HOAc forming an HB with the methoxy group. This path clearly indicates a strong basicity of OAc^- which would be able to deprotonate the nucleophile so that it could displace the substrate and attack directly the metal center, thus inactivating the catalyst. An estimate of the energy barrier for this deactivating path can be done from the energy of structure **B** with respect to the energy of $\mathbf{RC}_{\mathbf{OAc}}$, i.e. about 2.5 kcal/mol at DFT/BP86 level, which indicates that *if* $\mathbf{RC}_X$ *could be easily reached* this would be a facile process. However, the whole deprotonation path would start from $\mathbf{IC}_X$, which for OAc^- is 18.5 kcal/mol more stable than $\mathbf{RC}_{\mathbf{OAc}}$ at DFT/BP86 level, meaning that **B** would be 21.0 kcal/mol higher in energy than $\mathbf{IC}_{\mathbf{OAc}}$. Therefore, this deactivation pathway leading to the formation of the catalytically inactive species $\mathbf{DC}_X$ from $\mathbf{RC}_X$ can be ruled out for OAc^-, but not for TFA^-. In principle, TFA^- has a relatively strong proton acceptor capacity and, at the same time, the $\mathbf{RC}_{\mathbf{TFA}}$ is accessible. Interestingly enough, the 2-butyne is located in the second coordination sphere both in $\mathbf{IC}_{\mathbf{OAc}}$ and in structure **C**. Thus, alternatively, the $\mathbf{DC}_{\mathbf{OAc}}$ (or the $\mathbf{DC}_{\mathbf{TFA}}$) species could be generated in the pre-equilibrium step, before the substrate coordination to the catalyst takes place. In order to investigate this point, we considered the two ternary adducts depicted in Figure S1 for both OAc^- and TFA^-, and a transition state structure for the anion substitution by nucleophile has been calculated (see Figures S11 and S12). Indeed, the process leading to the methoxy inactivated species is feasible, with an activation energy barrier of 16.9 kcal/mol for OAc^- and 14.8 kcal/mol for TFA^-. This result is in agreement with the experimental observation that the reaction of the gold catalyst in the presence of OAc^- with methanol and in the absence of substrate is very slow (10% of acetic acid in 24 h), whereas in the presence of TFA^- it is faster (complete formation of TFAH after 3 h).

In the energy plot in Figure S8, there is a second transition state which can be reached from $\mathbf{RC}_{\mathbf{OAc}}$ by shortening the O−C1 distance to ca. 2.2 Å, which represents the transition state for the formation of the C−O bond (nucleophilic attack to butyne). The geometry optimization with O−C1 fixed at 2.2 Å and O−H at 1.6 Å gives the structure **D** shown in Figure 9. Then, the system proceeds to the vinyl ether intermediate product **I** (bottom, right corner in the plot) by only shortening the O−H distance (i.e., the hydrogen abstraction step follows the nucleophilic attack step). The geometry optimization with O−C1 fixed at 1.6 Å and O−H at 1.6 Å gives the structure **E** depicted in Figure 9, which indeed is close to the **I** structure. However, this process requires an even higher activation barrier (estimated value from the energy of structure **D** with respect to the energy of $\mathbf{RC}_{\mathbf{OAc}}$) of about 8.7 kcal/mol (at DFT/BP86 level) than that of the hydrogen abstraction from methanol. **D** would be 27.2 kcal/mol higher in energy than $\mathbf{IC}_{\mathbf{OAc}}$. We conclude that the strong coordinating ability of OAc^- is more responsible than the strong proton acceptor capacity for the lack of catalytic activity of the gold catalyst in the presence of the OAc^- anion. The strong coordinating power is related to the inability of acetate to form stable template character reactants complex $\mathbf{RC}_{\mathbf{OAc}}$. Since OAc^- requires a relatively high energy to hold the reactive methanol molecule in the right position for an outer-sphere addition, a concerted nucleophilic attack to butyne/nucleophile activation by anion cannot take place. On the other hand, the TFA^- strong proton acceptor character and less strong coordinating ability than OAc^- lead to the inactivation of the catalyst through the methoxy

DOI: 10.1021/cs501681f
ACS Catal. 2015, 5, 803−814

nucleophilic attack to gold and concomitant release of the substrate, as experimentally observed.[14]

CONCLUSION

In this paper we studied the role of the anion in the three main steps of the reaction mechanism of NHC gold(I)-catalyzed alkoxylation of alkynes, i.e. in the pre-equilibrium, nucleophilic attack, and protodeauration. We conclude that, compared to the bare $[NHCAu]^+$ catalyst, the anion greatly lowers the activation barrier of the protodeauration step acting as a proton shuttle, thus making the nucleophilic attack the rate-determining step.

However, in the first nucleophilic attack step, the anion can be responsible for two competing deactivation pathways of the catalyst.

The strong coordinating ability of the anion, which is commonly believed to be responsible for a scarce catalyst activity, is not the only reason for that, but also the combined strong proton acceptor capacity contributes to it.

This is the case for TFA^- and OAc^-. The lack of activity of OAc^- complex in the investigated catalytic process can be mainly attributed to its high coordinating affinity toward the cationic gold, which inhibits the reaction, preventing the alkyne coordination. Instead, the reduced catalytic efficiency of TFA^- complex can be mainly explained by its strong ability to accept the nucleophile proton and consequently to form free methoxy anion in solution which preferentially performs a nucleophilic attack to Au, thus inactivating the catalyst.

On the other hand, a weak coordinating ability and a poor proton acceptor capacity of the anion lead to an efficient catalyst only if the proton acceptor capacity can be enhanced by additional methanol molecules, as for BF_4^-. However, a relatively strong coordinating ability of the anion combined with a sufficiently good proton acceptor capacity yields an ideal catalyst, as for OTs^-. Hence, when an optimal balance between coordinating and proton acceptor abilities is realized, a more efficient catalyst can be obtained for gold catalyzed reactions where the nucleophilic attack is the rate-determining step.

These results rationalize well the experimentally observed catalytic activity, which varies in the order $OTs^- > BF_4^- > TFA^-$, with OAc^- showing no catalytic activity. Within this picture, the experimentally considered OTf^- anion, with coordinating and proton acceptor abilities intermediate between those of BF_4^- and OTs^-, can be predicted to have a catalytic efficiency which is also intermediate between those of BF_4^- and OTs^- in the investigated reaction, in agreement with the experimental results.[13,14]

This study highlights which are the important properties one should consider in selecting the correct anion for gold catalyzed alkoxylation of alkynes processes, as it can play a crucial role in determining the catalyst efficiency.

Clearly, the observed trend depends on the specific considered reaction and ligand (NHC). How the use of different substrates or ligands modifies the observed pattern is currently under investigation in our lab.

COMPUTATIONAL DETAILS

A comprehensive computational DFT[23,24] study was performed with ADF2013.01[25] program package to identify all the structures involved in the catalytic mechanism for different anions in the $[NHCAu]^+$ catalyzed addition of methanol to 2-butyne reaction (Scheme 2). For geometry optimizations, calculations were carried out at the DFT level of theory using the GGA functional BP86 (DFT/BP86).[26] Relativistic effects were treated with the scalar zero-order regular approximation, ZORA model.[27] All atoms were described with a Slater-type TZ2P triple-ζ quality basis set, using the frozen core approximation (1s for B, C, N, O, F; 2p for S; 4d for Au). Frequency calculations at the same BP86 level of theory have been also performed to identify all stationary points as minima (zero imaginary frequencies) or transition states (one imaginary frequency). All the two-dimensional plots of the energy have been calculated at BP86 level (DFT/BP86). Final energies have been calculated using ORCA program package[28] by single point B2PLYP perturbatively corrected doubly hybrid functional[29] calculations on the optimized BP86 gas phase structures in conjunction with a def2-TZVP basis set for all atoms and an ECP pseudopotential for gold to account for relativistic effects. This combined BP86 geometry optimization and B2PLYP energy calculation approach has been shown to give an high accuracy to describe gold species along reaction paths in benchmark studies (we refer to it as B2PLYP//BP86).[30] Unless otherwise specified, the B2PLYP functional is used for energy calculations. Due to the fact that the investigated reactions involve four molecules ($[NHC\text{-}Au]^+$, 2-butyne, methanol, and the anion X^-), the reference energy has been set to the most stable adduct involving all the molecules, in order to minimize entropy problems. Indeed, the entropic contribution to the reaction profile for OTs^- has been calculated for the two most different adducts (**NC** and **PC**) and they resulted identical in terms of translational contribution, very similar for the rotational one (0.04 entropic unit difference) and only with a small difference for the vibrational one (13 entropic units), as reported in the Supporting Information of our preliminary communication.[14]For this reason, computational mechanistic analysis is presented in enthalpy energies. All calculations were performed for the closed shell singlet state. For the same OTs^- reaction profile, calculations have been done including dispersion (B2PLYP-D3 functional) and solvent ($CHCl_3$) effects (B2PLYP/COSMO model) and comparable potential energy profiles have been found. All results are available as Supporting Information of our previous communication.[14]

ASSOCIATED CONTENT

Supporting Information

The following files are available free of charge on the ACS Publications website at DOI: 10.1021/cs501681f.

Additional Figures S1−S12 (PDF)

Cartesian coordinates of optimized structures in this work (ZIP)

AUTHOR INFORMATION

Corresponding Author

*Fax: +39 075 5855606. E-mail: paola.belanzoni@unipg.it.

Notes

The authors declare no competing financial interest.

ACKNOWLEDGMENTS

This work was supported by grants from the Italian MIUR and the FIRB-futuro-in-ricerca project: "Novel Au(I)-based molecular catalysts: from know-how to know-why (AuCat)", RBFR1022UQ.

DOI: 10.1021/cs501681f
ACS Catal. 2015, 5, 803−814

REFERENCES

(1) (a) Haruta, M. *Nature* **2005**, *437*, 1098−1099. (b) Nolan, S. P. *Acc. Chem. Res.* **2011**, *44*, 91−100.
(2) Fukuda, Y.; Utimoto, K. *J. Org. Chem.* **1991**, *56*, 3729−3731.
(3) Teles, J. H.; Brode, S.; Chabanas, M. *Angew. Chem., Int. Ed.* **1998**, *37*, 1415−1418.
(4) Gorin, D. J.; Sherry, B. D.; Toste, F. D. *Chem. Rev.* **2008**, *108*, 3351−3378.
(5) (a) Brouwer, C.; He, C. *Angew. Chem., Int. Ed.* **2006**, *45*, 1744−1747. (b) Schelwies, M.; Dempwolff, A. L.; Rominger, F.; Helmchen, G. *Angew. Chem., Int. Ed.* **2007**, *46*, 5598−5601. (c) Zhang, Z.; Widenhoefer, R. A. *Org. Lett.* **2008**, *10*, 2079−2081. (d) Weber, D.; Jones, T. D.; Adduci, L.; Gagné, M. R. *Angew. Chem., Int. Ed.* **2012**, *51*, 2452−2456. (e) Kovács, G.; Lledós, A.; Ujaque, G. *Organometallics* **2010**, *29*, 3252−3260.
(6) (a) Tarselli, M. A.; Chianese, A. R.; Lee, S. J.; Gagné, M. R. *Angew. Chem., Int. Ed.* **2007**, *46*, 6670−6673. (b) Xia, Y.; Dudnik, A. S.; Gevorgyan, V.; Li, Y. *J. Am. Chem. Soc.* **2008**, *130*, 6940−6941. (c) Davies, P. W.; Martin, N. *Org. Lett.* **2009**, *11*, 2293−2296. (d) Gorin, D. J.; Watson, I. D. G.; Toste, F. D. *J. Am. Chem. Soc.* **2008**, *130*, 3736−3737. (e) Gorin, D. J.; Watson, I. D. G.; Toste, F. D. *J. Am. Chem. Soc.* **2008**, *130*, 3736−3737.
(7) (a) Hamilton, G. L.; Kang, E. J.; Mba, M.; Toste, F. D. *Science* **2007**, *317*, 496−499. (b) LaLonde, R. L.; Sherry, B. D.; Kang, E. J.; Toste, F. D. *J. Am. Chem. Soc.* **2007**, *129*, 2452−2453.
(8) (a) Li, Z.; Brouwer, C.; He, C. *Chem. Rev.* **2008**, *108*, 3239−3265 and references therein; . (b) Jiménez-Nùnez, E.; Echavarren, A. M. *Chem. Rev.* **2008**, *108*, 3326−3350. and references therein. (c) Hashmi, A. S. K. *Chem. Rev.* **2007**, *107*, 3180−3211. (d) Krause, N.; Winter, C. *Chem. Rev.* **2011**, *111*, 1994−2009.
(9) Obradors, C.; Echavarren, A. M. *Chem. Commun.* **2014**, *50*, 16−28.
(10) Zhdanko, A.; Maier, M. M. *Angew. Chem., Int. Ed.* **2014**, *53*, 7760−7764.
(11) (a) Lein, M.; Rudolph, M.; Hashmi, A. S. K.; Schwerdtfeger, P. *Organometallics* **2010**, *29*, 2206−2210. (b) Kovács, G.; Ujaque, G.; Lledós, A. *J. Am. Chem. Soc.* **2008**, *130*, 853−864.
(12) (a) Zhdanko, A.; Maier, M. M. *Chem.—Eur. J.* **2014**, *20*, 1918−1930. (b) Roithovà, J.; Jankovà, Š; Jašikovà, L.; Vàňa, J.; Hybelbauerovà, S. *Angew. Chem., Int. Ed.* **2012**, *51*, 8378−8382. (c) Oonishi, Y.; Gómez-Suárez, A.; Martin, A. R.; Nolan, S. P. *Angew. Chem., Int. Ed.* **2013**, *52*, 9767−9771.
(13) Zhdanko, A.; Maier, M. E. *ACS Catal.* **2014**, *4*, 2770−2775.
(14) Biasiolo, L.; Trinchillo, M.; Belanzoni, P.; Belpassi, L.; Busico, V.; Ciancaleoni, G.; D'Amora, A.; Macchioni, A.; Tarantelli, F.; Zuccaccia, D. *Chem.—Eur. J.* **2014**, *20*, 14594−14598.
(15) (a) Bandini, M.; Bottoni, A.; Chiarucci, M.; Cera, G.; Miscione, G. P. *J. Am. Chem. Soc.* **2012**, *134*, 20690−20700. (b) Kim, J. H.; Park, S.-W.; Park, S. R.; Lee, S.; Kang, E. J. *Chem.—Asian J.* **2001**, *6*, 1982−1986.
(16) Zhow, T.; Xu, L.; Xia, Y. *Org. Lett.* **2013**, *15*, 6074−6077.
(17) Macchioni, A. *Chem. Rev.* **2005**, *105*, 2039−2074.
(18) (a) Wang, Y.; Wang, Z.; Li, Y.; Wu, G.; Cao, Z.; Zhang, L. *Nature Communication* **2014**, *5*, 3470 DOI: 10.1038/ncomms4470. (b) Marion, N.; Nolan, S. P. *Chem. Soc. Rev.* **2008**, *37*, 1776−1782.
(19) Wang, W.; Kumar, M.; Hammond, G. B.; Xu, B. *Org. Lett.* **2014**, *16*, 636−639.
(20) In the present work, the BAr^{F-} anion will not be considered because of its large size, its extremely low tendency to form ion pairs, and its inability to form HBs.
(21) Zuccaccia, D.; Bellachioma, G.; Cardaci, G.; Ciancaleoni, G.; Zuccaccia, C.; Clot, E.; Macchioni, A. *Organometallics* **2007**, *26*, 3930−3946.
(22) Krauter, C. M.; Hashmi, A. S. K.; Pernpointner, M. *ChemCatChem.* **2010**, *2*, 1226−1230.
(23) Schmid, T. M.; Consiglio, G. *Chem. Commun.* **2004**, 2318−2319.
(24) (a) Hohenberg, P.; Kohn, W. *Phys. Rev.* **1964**, *136*, B864−B871. (b) Kohn, W.; Sham, L. *J. Phys. Rev.* **1965**, *140*, A1133−A1138. (c) Parr, R. G.; Yang, W. In *Density-Functional Theory of Atoms and Molecules*; Oxford University Press: New York, 1989.
(25) (a) Baerends, E. J.; Ellis, D. E.; Ros, P. *Chem. Phys.* **1973**, *2*, 41−51. (b) Te Velde, G.; Bickelhaupt, F. M.; Baerends, E. J.; Guerra, C. F.; van Gisbergen, S. J. A. *J. Comput. Chem.* **2001**, *22*, 931−967. (c) *ADF User's Guide*, Release 2013.01, SCM, Theoretical Chemistry, Vrije Universiteit: Amsterdam, The Netherlands, 2013; http://www.scm.com.
(26) (a) Becke, A. D. *Phys. Rev. A* **1988**, *38*, 3098−3100. (b) Perdew, J. P.; Wang, Y. *Phys. Rev. B* **1986**, *33*, 8822−8824.
(27) (a) van Lenthe, E.; Baerends, E. J.; Snijders, J. G. *J. Chem. Phys.* **1994**, *101*, 9783−9792. (b) van Lenthe, E.; van Leeuwen, R.; Baerends, E. J.; Snijders, J. G. *Int. J. Quantum Chem.* **1996**, *57*, 281−293.
(28) Neese, F. *WIREs Comput. Mol. Sci.* **2012**, *2*, 73−78.
(29) Grimme, S. *J. Chem. Phys.* **2006**, *124*, 034108.
(30) (a) Ciancaleoni, G.; Rampino, S.; Zuccaccia, D.; Tarantelli, F.; Belanzoni, P.; Belpassi, L. *J. Chem. Theory Comput.* **2014**, *10*, 1021−1034. (b) Kang, R. H.; Chen, H.; Shaik, S.; Yao, J. *J. Chem. Theory Comput.* **2011**, *7*, 4002−4011. (c) Kang, R. H.; Lai, W.; Yao, J.; Shaik, S.; Chen, H. *J. Chem. Theory Comput.* **2012**, *8*, 3119−3127.

DOI: 10.1021/cs501681f
ACS Catal. 2015, 5, 803−814